Photoluminescence Properties of Zinc Oxide Film with Local Epitaxial Growth on Silicon Using Aluminum Nitride Buffer Layer

Liu Li, Liu Sha and Yang Yuan*

College of Petroleum and Chemical Engineering, BaYin GuoLeng Technology College, Xinjiang 841000, China

(Received November 19, 2019; revised version January 8, 2020; in final form January 28, 2020)

In this work, we report the preparation of zinc oxide (ZnO) film with local epitaxial growth on silicon substrate at room temperature using aluminium nitride (AlN) as buffer layer. ZnO and AlN films were deposited by RF and DC magnetron sputtering, respectively. The microstructures of c-axis oriented ZnO films deposited on (100) Si and AlN/Si substrates were studied by scanning electron microscopy, transmission electron microscopy, and X-ray diffraction. In addition, the effect of AlN buffer thicknesses (600 and 1400 nm) on photoluminescence properties of 400 nm thick ZnO deposits were also studied. Indeed, the deposition of ZnO on AlN buffer leads to a red shift of the band gap emission of ZnO compared to ZnO deposited without buffers. Moreover, the defects emission intensities and nature were also affected. The evolution of ZnO PL properties due to AlN buffer insertion is discussed with respect to the difference in the structural properties of ZnO film with and without AlN buffers.

DOI: 10.12693/APhysPolA.137.1110

PACS/topics: aluminium nitride, zinc oxide, buffer layer, photoluminescence, epitaxial growth

1. Introduction

Zinc oxide (ZnO) is an attractive II–VI semiconductor, with a direct band gap of about 3.3 eV and high exciton binding energy (60 meV) [1–3]. Therefore, it is suitable for optoelectronic devices, including ultraviolet-blue semiconductor lasers, light emitting diodes, and solar cells [1–4]. ZnO thin films have been grown using several deposition techniques, such as pulsed laser deposition [5], molecular beam epitaxy [6], MOCVD [7] etc. Furthermore, epitaxial growth of ZnO on silicon substrate (Si) is sometimes necessary in order to integrate these films in microelectronic devices. Nonetheless, due to the lattice mismatch between ZnO and Si, it is hard to grow epitaxial ZnO directly on Si substrate, at temperature compatible with that used in semiconductor technology. One possible way to overcome this limitation is by using a buffer layer with small lattice mismatch compared to that of ZnO. For instance, magnesium oxide (MgO) [8], gallium nitride [9], and aluminium nitride (AlN) [8, 10, 11], have been employed as buffer layers in order to obtain epitaxial growth of ZnO film. In particular AlN has a hexagonal wurtzite structure similar to that of zinc oxide, with lattice parameters of $a = 0.311$ nm and $c = 0.498$ nm [8]. On the other hand, ZnO has also hexagonal wurtzite structure, with lattice parameters of $a = 0.324$ nm and $c = 0.520$ nm [8]. Therefore, ZnO thin films can be grown on AlN by means of lattice-matching epitaxy, since the lattice misfit between these two materials is less than 4% [8]. Although, the epitaxial growth of ZnO has been reported in literature [8–11]. However, the optical properties of epitaxial ZnO are not well developed in literature. For example, very few studies have been reported on the photoluminescence (PL) performance of epitaxial ZnO. For example, Fujita et al. [12] have reported the PL emission intensity improvement of epitaxial ZnO deposited on MgO buffer layer. Xiong et al. [10] have also reported the PL improvement of grown ZnO on AlN buffer. In most of cases, the PL improvement of epitaxial ZnO is due to the structural quality improvement compared to ZnO deposited directly without epitaxial growth. However, epitaxial growth does not always lead to an enhancement of PL intensity, as it will be discussed in the present work.

In this work, we report on the epitaxial growth of ZnO thin films at low temperature ($< 100\,^{\circ}$C) on silicon substrates using an AlN buffer layer. The ZnO (400 nm thick) thin films were deposited by RF-sputtering on two AlN buffers with two different thicknesses of 600 nm or 1400 nm. We show that even for epitaxial ZnO, we did not obtain a significant improvement of band gap PL emission. In addition, the defect emissions were modified after AlN buffer insertion. The difference of PL signal before and after AlN insertion is discussed with respect to the structural modification of the ZnO deposit with and without AlN buffer. Our results add a piece of information for the optical properties of epitaxial ZnO film with specific structural configuration.

2. Experimental procedure

2.1. Deposition of AlN buffers

AlN films were deposited at room temperature, on (100) oriented silicon substrates, by reactive DC-sputtering in a customized reactor equipped with

*corresponding author; e-mail: 66299704@qq.com

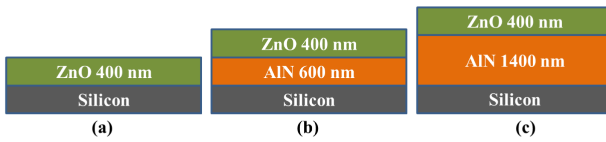

Fig. 1. Schematic design of the investigated samples. The ZnO films were grown on (a) silicon substrate, (b) 600 nm thickness AlN/silicon templates, (c) 1400 nm thickness AlN/silicon templates using RF-sputtering.

a 2 inch magnetron cathode, with a pure aluminium target at deposition pressure of 2 mTorr. Prior to deposition, the substrates were ultrasonically cleaned in acetone and ethanol, then dried under nitrogen gas flux. The sputtering target (aluminium) was 99.99% in purity with 2" in diameter, held on a water-cooled magnetron cathode. The distance between the target and substrate holder was 3 cm. The system was pumped to a base pressure of 4.5×10^{-5} Torr with a turbo-molecular pump before introducing argon (99.99%) and nitrogen (99.99%) gases. The total gas flux rate during deposition was maintained constant at 40 sccm while that of the reactive N_2 gas was fixed at 35%. The substrates were at floating potential and were not additionally heated nor cooled during the deposition. Deposition times of 20 min and 50 min were chosen, in order to obtain AlN buffer with two different thicknesses of 600 nm and 1400 nm, respectively.

2.2. *Deposition of ZnO*

Zinc oxide (ZnO) films were deposited on (100) silicon substrate and AlN (600 and 1400 nm thick) buffer layers, by RF-sputtering from 3" diameter of ZnO target. The target-sample distance was fixed at 2.6 cm. Argon (99.99%) as an inert gas was introduced through a mass flow controller. Sputtering deposition was performed under a gas pressure of 2.5 mTorr without intentional heating. The input power was kept at 200 W. The ZnO thickness (400 nm) was measured with a surface profilometer on silicon substrate loaded in the same reactor during ZnO deposition. The schematic structures of the samples are shown in Fig. 1. The samples are assigned as (a), (b) and (c) for ZnO deposited on Si without AlN buffer and for ZnO deposited on 600 nm and 1400 nm thick AlN buffers, respectively.

2.3. *Characterization tools*

The films were characterized by X-ray diffraction in θ–2θ scanning mode and by rocking curve mode on a D500 MOXTEK, using a Cu K_α radiation ($\lambda = 1.540598$ Å). The film cross-section observation performed by scanning electron microscopy (SEM) using a JEOL-type JSM 6400F at an accelerating voltage of 5 kV. The structural study of films was also carried out by high resolution transmission electron microscopy (HRTEM, Hitachi HF 2000), with an acceleration voltage of 200 kV. Photoluminescence (PL) measurements were collected on a Jobin-Yvon Fluorolog 3 spectrometer using a xenon lamp (500 W) with excitation wavelength = 300 nm, at room temperature.

Film thickness and substrate curvature were measured with a stylus profilometer DEKTAK 3030. As most commonly used, the stress in our films has been calculated by the bend-bending method, where the radius of the coated substrate curvature is determined and used to calculate the residual stress. The internal stress in the deposited film is calculated from the change in the substrate curvature from $1/R_0$ for the uncoated substrate to $1/R_e$ after film deposition, with the following Stoney formula [13]:

$$\sigma = \frac{(E_s e_s^2)}{6e(1-\nu_s)}\left(\frac{1}{R_e} - \frac{1}{R_0}\right),$$

where R_0 is the radius of curvature of the Si substrate, R_e is the curvature radius after film deposition, E_s and ν_s are, respectively, the Young modulus and Poisson ratio of the substrate, e_s and e are the thickness of the substrate and the film, respectively.

3. Results and discussions

3.1. *Structural and morphological characterization*

Figure 2a,b presents the XRD patterns of 400 nm ZnO film deposited on silicon substrate and AlN buffers (600 nm and 1400 nm thick). The X-ray diffraction

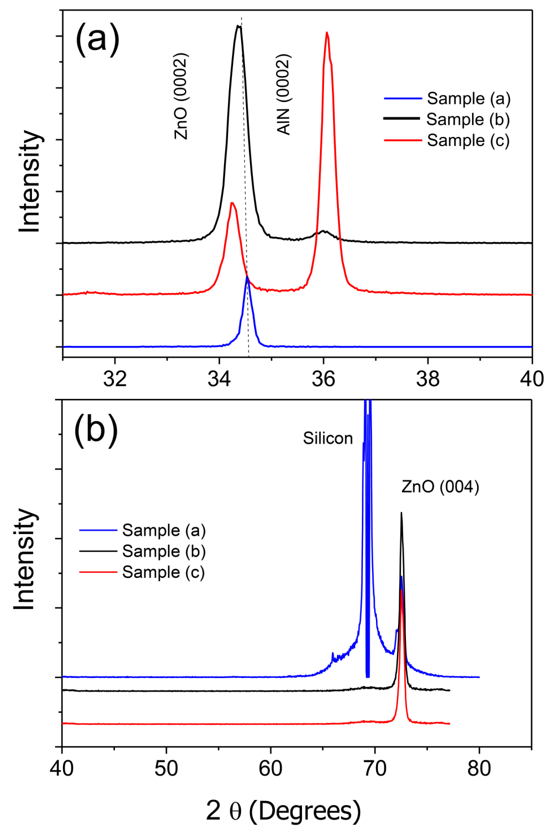

Fig. 2. XRD patterns of the ZnO films grown on silicon substrate and different AlN buffer layers (a) from 2θ30–40° and (b) extended interval from 40–80°.

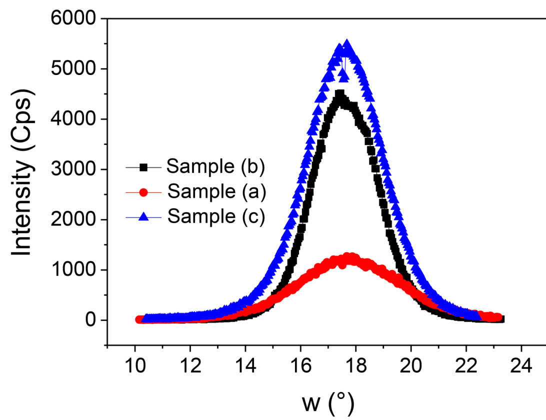

Fig. 3. The high-resolution XRD (0002) w-scan rocking curves of ZnO films grown on (a) silicon substrate, (b) 600 nm thick AlN buffer, and (c) 1400 nm thick AlN buffer.

(XRD) results reveal a remarkable crystallization of ZnO (0002) on AlN (0002) [1–3, 10]. Indeed, such result is confirmed by the FWHM of the (0002) ZnO in rocking curve (RC) mode (in Fig. 3), which is 4.3° for ZnO on Si and 2.9° and 2.4° on 600 nm thick and 1400 nm thick AlN buffers, respectively. The extended XRD pattern (Fig. 2b) confirms the single orientation of ZnO deposited with and without the buffer layer. Moreover, one can observe an important shift of the ZnO (0002) diffraction peak from 34.53° to 34.37° and 34.25°, for samples a, b, and c, respectively. This indicates a change in the stress, which is compressive on Si and tensile on AlN. Such change in stress could have an impact on the optical properties of ZnO films. The stress calculated using Stoney's formula [13] was found to be −0.7749 GPa for ZnO/Si (sample a) and −0.6151 GPa and −0.4896 GPa for sample b and c, respectively. This implies that the stress of ZnO deposit is compressive on silicon, while the stress becomes tensile for ZnO deposited on AlN buffers.

Figure 4a, b shows the cross-section SEM images of ZnO film deposited on Si and 1400 nm thick AlN buffer layer, respectively. The ZnO/Si film exhibits a dense and compact surface morphology compared to ZnO grown on AlN buffer. Indeed, the ZnO grown on 1400 nm thick AlN adopts a columnar structure, which in fact seems to be a continuous growth of the AlN buffer, which has already a columnar structure. The same structure of ZnO with columnar structure is also obtained for 600 nm thick AlN (not shown here). This is consistent with XRD results since both ZnO and AlN films have both a wurtzite structures with (0002) orientation.

In order to have an insight on the continuous growth of ZnO on AlN buffer, TEM was performed on ZnO deposited on 1400 nm thick AlN buffer. It should be noted that the same results were observed in the case of ZnO deposited on 600 nm thick AlN buffer (not shown here). The TEM micrograph of ZnO film deposited on the AlN buffer is displayed in Fig. 5a. In this figure, is it clear that

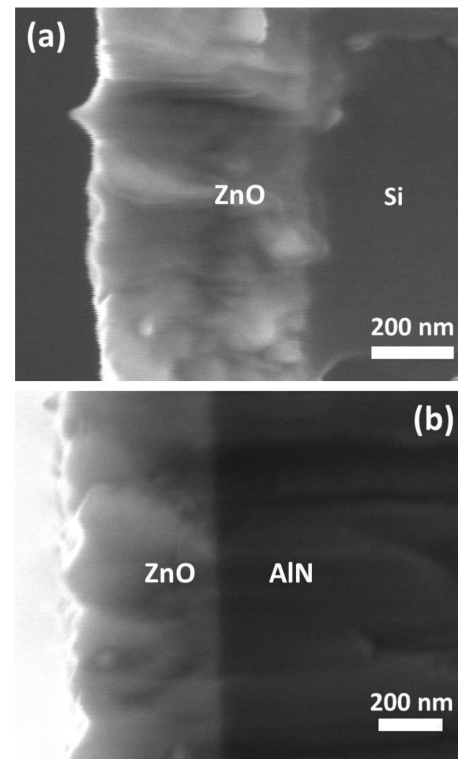

Fig. 4. Cross-section SEM images of ZnO deposited on (a) silicon and (b) 600 nm thick AlN buffer.

ZnO has a kind of continuous growth with well-aligned columns which are superposed on those of AlN buffer. The HRTEM image (Fig. 5b) of the rectangular part in Fig. 5a shows a kind of epitaxial growth of ZnO on AlN buffer with an interface that appears relatively abrupt. Such epitaxial growth is emphasized in Fig. 5c which is a high resolution of rectangular part in Fig. 5b. Indeed, the interface between ZnO film and AlN buffer is clearly abrupt, indicating a local epitaxial growth of ZnO on the AlN buffer. The electron diffraction patterns labelled 1, 2 and 3 on AlN, the interface between ZnO/AlN and ZnO film, respectively, confirm the single crystalline epitaxial nature of zinc oxide growth on AlN. In fact, well-aligned spots are observed in the SAED pattern of the interface ZnO/AlN which are identical to those obtained for AlN or ZnO films. The sputtered ZnO film at the interface appears to be well crystallized and fully c-axis orientated. It is worth to notice that the ion bombardment had not destroyed the AlN crystalline structure during the beginning of ZnO growth thanks to AlN extreme resistance to amorphization during ion irradiation due to efficient dynamic defect annihilation [14].

3.2. Photoluminescence measurements

In order to evaluate the effect of AlN buffer layer on the PL properties of ZnO, we first measured the PL properties of ZnO deposited directly on Si substrate without buffer. Figure 6 shows the PL spectra of ZnO thin film

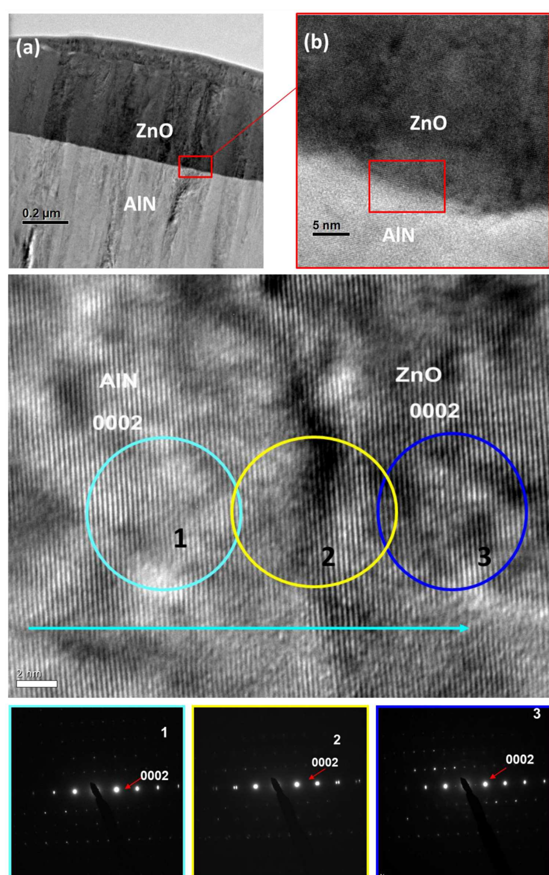

Fig. 5. TEM micrograph of ZnO film deposited on 1400 nm thick AlN buffer, (b) High resolution TEM image of the rectangular part of (a). The inset is the SAED of the rectangular part in (a). (c) High resolution TEM image of the rectangular part in (b).

grown on Si substrate. In Fig. 6, the strong peak at 389 nm (3.19 eV), corresponds to the band-edge emission of the ZnO due to recombination of excitons bound to donors [15, 16]. The emission peaks at 411, 431, 500, 545 nm [17–19] can be ascribed to the intrinsic point defect, such as zinc vacancy, zinc interstitials, or oxygen vacancies [20]. However, these peaks may also originate from interference effects with the silicon layer. The spacing observed between them is about 40 nm, which roughly corresponds to interference fringe spacing found for 1000 nm thick ZnO deposited on Si [21]. Indeed, these fringe spacings are due to the Fabry–Pérot oscillations that will be formed when a thin film is deposited on a smooth and refractive substrate. Multiple optical reflections occur due to differences in the refractive indices of the ZnO films, substrates, and the ambient (air in the present study) [21]. It must be noted that PL spectra free of fringe spacings have been reported in the case of ZnO films thinner than 70 nm or much thicker than 1.5 μm, which is not our case since our films have thickness of 400 nm. In addition, when a thick buffer layer of AlN is used, these peaks are not observed as it will be shown hereafter.

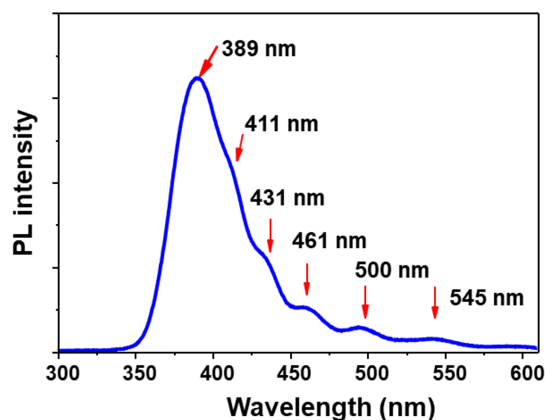

Fig. 6. Room temperature PL spectrum from ZnO thin film grown on Si substrate without a buffer layer.

It is also reported that the defect emissions depend on the fabrication process of ZnO [22]. Transient PL spectra of ZnO film grown on Si substrate with different buffer layer (AlN) thicknesses of 600 and 1400 nm are shown in Fig. 7a,b. In Fig. 7a, a strong UV emission at 392 nm (3.16 eV) can be assigned to the near band-edge transition in ZnO. The FX mode which is usually situated at 375.7 nm (3.3 eV) was not observed here [22] and therefore, any of its replicas FX-LO and FX-2LO, (band which is the free exciton (FX) and coupling of FX with orders of longitudinal optical (LO) phonon replicas) can be ruled out, even the FX-2LO is reported to be situated between 395 and 392 nm [23].

In addition, strong and weak emissions at 432 and 512 nm, respectively, are observed in the case of ZnO deposited on 600 nm thick AlN buffer. Assuming that interference effects can be neglected here [21], these peaks may come from intrinsic point defects, such as zinc interstitials and oxygen vacancies [22–24], respectively. Concerning the emission, at 432 nm (2.8 eV) for ZnO/AlN (600 nm) it may originate from defect emission in ZnO [25, 26] or synergistic effect between ZnO and AlN defects. In fact, a transition between the complexes of Al vacancies and oxygen on a nitrogen site in AlN and the Zn vacancies defect states in ZnO has been reported to be about 2.9 eV [27], which is close to 2.8 eV in our case.

The PL of ZnO deposited on thicker AlN buffer of 1400 nm manifest a strong and broad UV emission at 392.3 nm (equivalent to 3.16 eV) as shown in Fig. 7b, which indicates a decrease of the ZnO band gap [28]. One can notice from the PL spectra that the insertion of AlN buffer leads to red shift of UV emission by 4 nm and 4.3 nm for 600 nm and 1400 nm thick AlN buffers, respectively, suggesting a band gap decrease of ZnO when using AlN buffers. This can be attributed to stress effect in ZnO due to AlN buffer insertion [29]. Indeed, it has been demonstrated that the upward shift in the energy bandgap corresponds to the occurrence of compressive stress in the ZnO crystal [30], while a band-gap decrease is due to tensile stress [31]. This is consistent with the

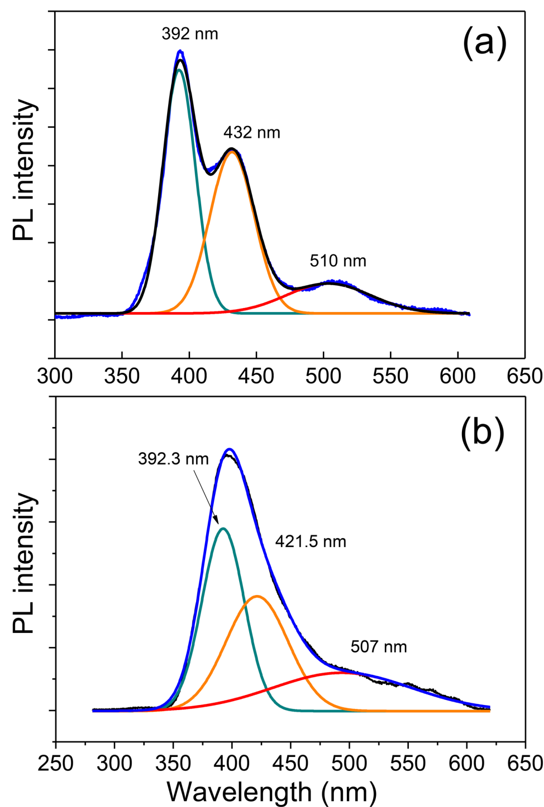

Fig. 7. Deconvoluted room temperature PL spectra from ZnO thin film grown on Si substrate with a buffer layer (a) 600 nm, (b) 1400 nm.

XRD results, where an increase in tensile stress is observed due to AlN buffer insertion. In addition, the defect emission (situated around 507 nm) of the ZnO deposited on 1400 nm thick AlN is broader than the other peaks from the ZnO/Si and ZnO/AlN (600 nm) film, which is related to the defects that can originate from the void between columns [32]. It is worth to mention that the rocking curve measurements show only the orientation of ZnO in (0002) direction and do not give information about the other type of defects.

Finally, although, there is a local epitaxial growth of ZnO on AlN buffers, the defect emission that are originated from ZnO, or AlN buffer or both were also present. In addition, no significant improvement of the band gap emissions were measured for films deposited on AlN buffers. Indeed, the local epitaxial growth was a kind of continuous local growth of the ZnO columns on those of AlN buffer as already shown in SEM/TEM images, thus, the ZnO deposited on AlN became less dense compared to ZnO deposited directly on Si.

4. Conclusions

Epitaxial and *c*-axis oriented ZnO films were grown on AlN/Si(100) substrate by RF magnetron sputtering at low temperature ($< 100\,^{\circ}$C), which is an easy technique compatible with the current semiconductor technology. The PL results were somehow out of the traditional thought box, which supposes that epitaxial growth would enhance the band gap emission of ZnO. The local epitaxial growth in our case was in the form of a continuous growth of ZnO columns on those of AlN, which led to less dense structure compared to that of ZnO grown directly on Si. This results to the appearance or increase of new defects such as zinc interstitials, thus, the PL signal was broadened and some defect emissions were enhanced. In addition, the defect from AlN buffer cannot be ruled out. Our results add a piece of information about the PL properties of ZnO with local epitaxial growth on AlN buffer.

Acknowledgments

This work was supported financially by School of Chemistry and Chemical Engineering, Shihezi University/Key Laboratory for Green Processing of Chemical Engineering of Xinjiang Bingtuan/Key Laboratory of Materials-Oriented Chemical Engineering of Xinjiang Uygur Autonomous Region/ Engineering Research Center of Materials-Oriented Chemical Engineering of Xinjiang Bingtuan, Beisi Road, Shihezi 832003, Xinjiang, People's Republic of China.

References

[1] F.E. Ghodsi, H. Absalan, *Acta Phys. Pol. A* **118**, 659 (2010).

[2] D. Gültekin, M. Alaf, H. Akbulut, *Acta Phys. Pol. A* **123**, 274 (2013).

[3] H. Eskalen, S. Ozan, U. Alver, S. Kerl, *Acta Phys. Pol. A* **127**, 756 (2015).

[4] W. Li, Y-X. Xu, D. Wang, F. Chen, Z-K. Chen, *Org. Electron.* **57**, 60 (2018).

[5] Y. Zeng, Y. Zhao, Y. Jiang, *Surf. Interface Anal.* **46**, 602 (2014).

[6] S.P. Wang, C.X. Shan, B. Yao, B.H. Li, J.Y. Zhang, D.X. Zhao, D.Z. Shen, X.W. Fan, *Appl. Surf. Sci.* **255**, 4913 (2009).

[7] N.M. Sbrockey, S. Ganesan, *III–Vs Review* **17**, 23 (2004).

[8] C. Jin, R. Narayan, A. Tiwari, H. Zhou, A. Kvit, J. Narayan, *Mater. Sci. Eng. B* **117**, 348 (2005).

[9] A. Nahhas, H.K. Kim, J. Blachere, *Appl. Phys. Lett.* **78**, 1511 (2001).

[10] H. Xiong, J.N. Dai, Xiong Hui, Y.Y. Fang, W. Tian, D.X. Fu, C.Q. Chen, Mingkai Li, Yunbin He, *J. Alloys Compd.* **554**, 104 (2013).

[11] K. Kondo, M. Harada, N. Shibata, *J. Ceram. Soc. Japan* **110**, 343 (2002).

[12] M. Fujita, N. Kawamoto, M. Sasajima, Y. Horikoshi, *J. Vacuum Sci. Technol. B* **22**, 1484 (2004).

[13] J. Singh, S. Ranwa, J. Akhtar, M. Kumar, *AIP Adv.* **5**, 067140 (2015).

[14] J.S. Williams, *Mater. Sci. Eng. A* **253**, 8 (1998).

[15] A. Sasaki, W. Hara, A. Matsuda, N. Tateda, S. Otaka, S. Akiba, K. Saito, T. Yodo, M. Yoshimoto, *Appl. Phys. Lett.* **86**, 231911 (2005).

[16] V. Pawar, P.K. Jha, S.K. Panda, P.A. Jha, P. Singh, *Phys. Rev. Appl.* **9**, 054001 (2018).

[17] B. Lin, Z. Fu, Y. Jia, *Appl. Phys. Lett.* **79**, 943 (2001).

[18] Q.X. Zhao, P. Klason, M. Willander, H.M. Zhong, W. Lu, J.H. Yang, *Appl. Phys. Lett.* **87**, 211912 (2005).

[19] N.O. Korsunska, L.V. Borkovska, B.M. Bulakh, L.Y. Khomenkova, V.I. Kushnirenko, I.V. Markevich, *J. Lumin.* **102**, 733 (2003).

[20] A. Achour, M. Islam, S. Vizireanu, I. Ahmad, M.A. Akram, K. Saeed, G. Dinescu, J.-J. Pireaux, *Nanomaterials* **9**, 794 (2019).

[21] Y.-G. Wang, N. Ohashi, H. Ryoken, H. Haneda, *J. Appl. Phys.* **100**, 114917 (2006).

[22] Y. Gong, T. Andelman, G.F. Neumark, S. O'Brien, I.L. Kuskovsky, *Nanoscale Res. Lett.* **2**, 297 (2007).

[23] U. Choppali, B.P. Gorman, *Opt. Mater.* **31**, 143 (2008).

[24] M.A. Hashmi, K. Mahmood, A. Alib, M. Hasan, M. Raja, I. Hussain, M. Willander, *ECS Trans.* **35**, 149 (2011).

[25] M.K. Patra, K. Manzoor, M. Manoth, S.R. Vadera, N. Kumar, *J. Lumin.* **128**, 267 (2008).

[26] D.H. Zhang, Z.Y. Xue, Q.P. Wang, *J. Phys. D Appl. Phys.* **35**, 2837 (2002).

[27] J. Ding, H. Chen, H. Fu, *Mater. Res. Bull.* **95**, 185 (2017).

[28] Munirah, Z.R. Khan, A. Aziz, M.S. Khan, M.U. Khandaker, *Mater. Sci.-Poland* **35**, 243 (2017).

[29] V. Venkatachalapathy, A. Galeckas, I.-H. Lee, A.Yu. Kuznetsov, *Physica B Condens. Matter* **407**, 1476 (2012).

[30] T. Prasada Rao, M.C. Santhosh Kumar, S. Anbumozhi Angayarkanni, M. Ashok, *J. Alloys Compd.* **485**, 413 (2009).

[31] R.K. Sendi, S. Mahmud, *J. Phys. Sci.* **24**, 1 (2013).

[32] M.S. Kim, K.G. Yim, J.-Y. Leem, *J. Korean Phys. Soc.* **59**, 2354 (2011).